

RESEARCH

Open Access



# Variable cross-sectional effect on bi-directional blades–tower–soil–structure dynamic interaction on offshore wind turbine subject to wind–wave loads

Mostafa A. El Absawy<sup>1\*</sup> , Zakaria Elnaggar<sup>1</sup>, Hesham H. Ibrahim<sup>2</sup> and M. H. Taha<sup>1</sup>

## Abstract

**Background** This study introduces a numerical model designed to simulate interactions occurring between a wind turbine's tower and the surrounding soil, as well as between the nacelle, blades, and the surrounding environment. This simulation accounts for both fore–aft and side-to-side movements. To describe these interactions, the model leverages the Euler–Lagrange equations. It calculates wave loads utilizing the Morison equation, with wave data generated based on the JONSWAP spectrum. Furthermore, aerodynamic loads are determined using the blade element moment theory, and the wind spectrum is generated using the Von Karman turbulence model. The tower is represented as a variable cross-sectional beam, employing a two-noded Euler beam element with two degrees of freedom: transverse displacement and rotation, and utilizing Hermite polynomial shape functions.

**Results** In a comparative analysis against experimental data, this modified model demonstrates significant enhancements in accurately reproducing the dynamic behavior of wind turbines with variable cross-sectional towers, outperforming models that approximate the tower with a constant cross section. Our findings reveal that the modified model achieves a remarkable improvement of 15% in replicating the tower's dynamic response when compared to the constant cross-sectional models. As a case study, a 5 MW monopile wind turbine with a flexible foundation, specifically the one provided by the National Renewable Energy Laboratory (NREL), is employed to simulate its dynamic response.

**Conclusions** This research presents a robust numerical model for simulating wind turbine behavior in various environmental conditions. The incorporation of variable cross-sectional tower representation significantly improves the model's accuracy, making it a valuable tool for assessing wind turbine dynamics. The study's findings highlight the importance of considering tower flexibility in wind turbine simulations to enhance their real-world applicability.

**Keywords** Wind turbine, Numerical model, Variable cross-sectional tower, Euler–Lagrange equations, Morison equation, JONSWAP spectrum, Blade element moment theory, Von Karman turbulence model, Flexible foundation, Dynamic response

\*Correspondence:

Mostafa A. El Absawy  
maselabsawy\_2011@cu.edu.eg

<sup>1</sup> Department of Engineering Mathematics and Physics, Faculty of Engineering, Cairo University, Giza, Egypt

<sup>2</sup> Department of Mechatronics, Engineering and Material Sciences School, German University, Cairo, Egypt

## 1 Background

The present global political and economic landscape has led to a shift in the scientific community's focus toward renewable energy sources. This shift is primarily driven by escalating costs and the diminishing reserves of fossil fuels. Many nations have devised medium- and



© The Author(s) 2023. **Open Access** This article is licensed under a Creative Commons Attribution 4.0 International License, which permits use, sharing, adaptation, distribution and reproduction in any medium or format, as long as you give appropriate credit to the original author(s) and the source, provide a link to the Creative Commons licence, and indicate if changes were made. The images or other third party material in this article are included in the article's Creative Commons licence, unless indicated otherwise in a credit line to the material. If material is not included in the article's Creative Commons licence and your intended use is not permitted by statutory regulation or exceeds the permitted use, you will need to obtain permission directly from the copyright holder. To view a copy of this licence, visit <http://creativecommons.org/licenses/by/4.0/>.

long-term strategic plans that prioritize the development and integration of green energy sources in the upcoming decades. Furthermore, recent international climate conferences have underscored the imperative of increased investments in clean energy technology to mitigate greenhouse gas emissions. Wind energy stands out as a remarkably efficient resource within the realm of renewable energy, chiefly due to its cost-effectiveness and wide availability. Among the various wind energy technologies, offshore wind turbines (OWT) have garnered significant attention due to their exceptional energy density. However, despite the evident advantages of OWT when compared to onshore turbines, there remains a crucial need for further research concerning their maintainability, as well as their impact on operational conditions and longevity. This research is vital to optimizing the performance of offshore wind turbines and ensuring the enduring sustainability of this technology. The study of the dynamic behavior of offshore wind turbines (OWT) is a multifaceted and complex subject that encompasses various research areas. These areas include the modeling of the entire wind turbine, the tower (utilizing continuous-multi step or uniform-variable cross-sectional methods), the interaction between the structure and the soil (involving springs, dampers, combinations thereof, or piles), the nacelle–blades system (considering multi-blades, nacelle with gearbox, or simplified mass representations, depending on the study's objectives), and the primary direction of analysis (uni-directional, bi-directional, or torsional). These research domains are essential for gaining a comprehensive understanding of OWT's performance and for optimizing its long-term sustainability. The process of modeling the dynamic behavior of OWT commences with the determination of the fundamental natural frequencies, which provides critical insights into the turbine's behavior. Using these fundamental characteristics as a foundation, simulations are conducted to predict the loads acting on the wind turbine. These loads encompass seismic, hydrodynamic, and aerodynamic forces. The response of various components of the wind turbine is obtained by solving the governing equations used in the modeling process. Based on the acquired responses, improved designs can be proposed through optimization techniques. These optimizations may involve adjustments to blade characteristics, tower dimensions, or the implementation of specific control methods to manage the turbine's response effectively. A substantial body of research is readily accessible concerning the dynamics of wind turbines. This extensive body of work encompasses various facets, such as the dynamics of individual components, their interactions, and the identification of pivotal factors that hold significance. Moreover, a wide array of mathematical and

experimental techniques have been proposed to enhance the precision of modeling, all while maintaining computational and experimental efficiency. The overarching goal of these studies has been to furnish a more comprehensive comprehension of wind turbine dynamic behavior and to facilitate the optimization of its performance, ensuring its long-term sustainability.

Thresher [1] conducted a comprehensive review of various methods used to dynamically simulate horizontal-axis turbines in comparison to experimental data. Halfpenny [2] developed an innovative frequency domain model suitable for analyzing both offshore and onshore wind turbines with full flexibility, utilizing the finite element technique. These studies have provided valuable insights into the dynamic behavior of wind turbines and the simulation methods employed, which can contribute to the development of enhanced wind turbine system designs. Ahlstrom [3] delved into the aeroelastic dynamic responses of horizontal-axis turbines by developing a finite element model. Kessentini et al. [4] employed the differential quadrature method (DQM) to create a mathematical model for horizontal-axis turbines with elastic blades and towers, accounting for structural damping and nacelle pitch angles. As this current research specifically focuses on the dynamic interactions between the tower, blades, and nacelle in offshore wind turbines with elastic foundations, we will provide a brief overview of the literature that addresses various aspects related to this topic in the following sections.

Molenaar [5] conducted an extensive review of the theoretical foundations and design possibilities related to wind turbine dynamics, including the dynamics of offshore turbines influenced by waves. Oh et al. [6] conducted a review of various types of wind turbine foundations and the different modeling techniques used to analyze the interaction between the structure and the soil. These studies offer valuable insights and information on various aspects of wind turbine dynamics, including offshore wind turbine foundations and wave effects, which can contribute to the development of improved wind turbine system designs.

Xu et al. [7] utilized finite element analysis to investigate the dynamic and static behaviors of a tower supporting a 600 KW wind turbine, while considering the influence of flexible subgrade soils. Bhattacharya and co-authors [8] summarized findings from a series of 1:100 scale tests of a V120 Vestas turbine supported by two types of foundations: monopiles and tetrapod suction caissons. These outcomes provided valuable insights into long-term performance and issues related to structure–soil interaction. Adhikari and Bhattacharaya [9] presented a closed-form approximate model for estimating the fundamental frequency of wind turbine towers

with elastic foundations. The proposed analytical design is based on the theory of Euler–Bernoulli beam columns with flexible end supports. Bhattacharaya and Adhikari [10] introduced innovative experimental procedures for obtaining the parameters required for the dynamic modeling of offshore wind turbines. Their results indicated significant variations in the damping factors and natural frequencies of wind turbine towers depending on the foundation–soil interaction model. Arany et al. [11] developed an analytical model for offshore wind turbines with elastic foundations to obtain a rapid and relatively accurate estimation of the fundamental frequency. This model is suitable for initial design or for confirming results obtained using finite element analysis. Alamo et al. [12] investigated the dynamic impact of foundation constraints on offshore wind turbines, highlighting the influence of soil–structure interaction on the accuracy of the assessed fundamental frequency and the corresponding soil–structure system damping. Kumar and Nasar [13] studied the dynamic behavior of offshore wind turbines subjected to rotor-induced and environmental vibration forces using an Euler–Bernoulli beam-column model with flexible end supports for the tower. Subsequently, Wang et al. [14] conducted an in-depth investigation of wind turbine dynamics by incorporating an enhanced model that considered vibration signal analysis and employed the Euler–Lagrangian approach. This approach allowed for the consideration of dynamic interactions between the nacelle–tower and the tower–foundation system. Bouzid et al. [15] developed a computational methodology that employed nonlinear finite element analysis to simulate the dynamic characteristics of monopile foundations for offshore wind turbines, with a particular focus on incorporating foundation flexibility as a crucial aspect of the model.

Negm and Maalawi [16] utilized an optimization model that conceptualizes the wind turbine tower as a series of fixed, uniform, round tubular segments, incorporating a top mass to simulate the nacelle–blade system. The forces, including aerodynamic, gravitational, and inertial forces, are distributed along the tower within an undeformed inertial coordinate system. Murtagh et al. [17] proposed a model for a wind turbine under prolonged wind loading, representing the turbine as a tower with a top mass encompassing the blade/nacelle system. The applied load is divided into two components: a drag force affecting the tower and a force affecting the top mass, derived from the rotation of the blades treated as cantilever beams subjected to gravity and centrifugal forces. However, this model does not consider soil–structure or blade–tower interactions. Mohammad AlHamaydeh and Saif Hussain [18] employed three-dimensional finite element analysis using SAP2000 software to model

a pile–tower–foundation system constructed of reinforced concrete, incorporating a top mass. The model accounts for wind loads under both steady and unsteady conditions, and it is represented as a single-degree-of-freedom (SDOF) system. John Arrigan et al. [19] investigated the variation in blade natural frequency due to changes in blade rotation and stiffness to reduce flapwise vibration through the use of semi-active tuned mass dampers (STMD). The model considers three uniformly cantilevered beams with mass at the root, representing the nacelle and accounting for blade–tower interaction. Arturo Soriano et al. [20] conducted a comprehensive review of nonlinear and linear techniques for dynamic modeling of wind turbines, including actuators, and explored various control methodologies, including nonlinear ones. Liu [21] analyzed the tower–cabin–blade coupling system for wind turbines, establishing the coordinate system and motion equation as a single-degree-of-freedom (SDOF) system. Genov et al. [22] developed a model for a wind turbine experiencing random aerodynamic load, with the tower represented as a viscously damped fixed-bottom beam with a top mass for the nacelle/blade system. The model includes four equations accounting for various dynamic aspects. Fitzgerald and Basu [23] proposed a multi-degree-of-freedom (MDOF) model using the Euler–Lagrangian method, considering interactions between out-of-plane and in-plane blade vibrations and exploring the significance of structure–soil interaction in wind turbine control. Zuo et al. [24] introduced a 3D finite element model for a 5 MW turbine from the National Renewable Energy Laboratory (NREL) subjected to wind, sea wave, and seismic loads, focusing on the tower while excluding the blades from the scope. Staino and Basu [25] proposed a novel control technique merging active tendon and passive pitch controls, using a fixed tower model with bi-directional blade and tower vibrations and considering three types of loads: wind, gravity, and rotor acceleration. Mohammadi et al. [26] employed an adaptive control algorithm to cancel vibration signals after identifying their frequencies in a fixed tower structure, utilizing multiple software codes for different aspects of wind energy system simulation. Hussan et al. [27] summarized methods to reduce jacket vibration in offshore wind turbines exposed to wind, waves, and seismic loads, incorporating multiple tuned mass dampers (MTMDs). Sun [28] explored the control of a wind turbine exposed to wave, seismic, and wind loads using a semi-active tuned mass damper (STMD), with a focus on uni-directional tower vibration and bi-directional blade vibration. Hemmati and Oterkus [29] proposed a model for an OWT considering time-varying STMD and damage conditions, including nonlinear soil–pile interaction. Brodersen et al. [30] applied an active tuned mass

damper (ATMD) to a fixed wind turbine tower. Hsu [31] utilized the differential quadrature method to represent the dynamic behavior of rotating wind turbine blades. Park et al. [32] investigated the modal characteristics of rotating blades and examined frequency variations with changes in blade rotation speed. Li et al. [33] developed a nonlinear model for wind turbine blade vibrations, considering longitudinal, in-plane bending, out-of-plane bending, and torsion vibrations, accounting for damping and moment and force distributions on the blade section. Kono et al. [34] studied the upwind influence on wind turbine towers using computational fluid dynamics (CFD) simulations, with a specific focus on tower behavior. El Mouhsine et al. [35] optimized wind turbine blade shapes based on aerodynamic and structural analysis. Júnior et al. [36] evaluated the performance of nonlinear large deformation blade models, including three-dimensional shell finite elements and exact beam models, for both static and dynamic analysis.

Expanding upon the research conducted by El Absawy et al. [37, 38], a multi-degree-of-freedom (MDOF) model has been developed for dynamic analysis of offshore wind turbine towers characterized by varying cross-sectional geometries and elastic foundations. This model takes into consideration the interplay between the tower, nacelle, and blades in both lateral (side-to-side) and longitudinal (fore-and-aft) directions. The proposed model represents the interaction between the structure and the soil by incorporating longitudinal, coupled, and rotational spring–damper elements in both lateral and longitudinal directions. Blade dynamics are modeled by accounting for centrifugal stiffness, bending stiffness, and gravitational effects. Wave loading is assessed using the Morison equation, with wave data generated based on the JON-SWAP spectrum. Aerodynamic loads are calculated using the blade element moment theory, while the wind spectrum is generated through the Von Karman turbulence model. The nonlinear governing equations are derived using an Euler–Lagrangian energy-based approach and solved using the Newmark procedure. The impact of the varying cross-sectional geometry of the tower is compared with that of a tower with a constant cross-sectional shape for further analysis.

## 2 Methods

### 2.1 Physical model

The research focuses on a 3D wind turbine system comprising a tower, nacelle, and blades. The system has varying cross sections and an elastic foundation. It faces random wave and wind turbulence loads. Wave load is misaligned with the wind direction, represented by  $\beta$ . The tower is an Euler beam, and the nacelle contains rotating blades. The

coordinate system is based at the tower’s center line and the soil level intersection (Fig. 1).

The three blades coordinate  $q_1–q_3$  denotes the edgewise coordinates in Fig. 2a and  $q_4–q_6$  denotes the flapwise coordinates in Fig. 2b. The rotating blades speed is  $\Omega$  in which the blades angle  $\psi_i$  of the  $i$ th blade is given by:

$$\psi_i(t) = \Omega t + \frac{2\pi}{3}(i - 1), \quad i = 1, 2, 3 \quad (1)$$

Nacelle’s relative motion represented by  $q_7$  (fore–aft) and  $q_8$  (side–side). Soil–structure interaction (SSI) is modeled by springs ( $k_{lx}, k_{ly}, k_{rx}, k_{ry}, k_{xy}$ ) and dashpot dampers ( $c_{lx}, c_{ly}, c_{rx}, c_{ry}$ ). OWT is MDOF with 12 DOFs. Blades have six DOFs (flapwise, edgewise). SSI is indicated by four DOFs:  $q_9–q_{11}$  (translation),  $q_{10}$  and  $q_{12}$  (rotation).

### 2.2 Mathematical model (Euler–Lagrangian equation)

The model is expressed utilizing the Euler–Lagrangian energy-based method:

$$\frac{d}{dt} \frac{\partial T(t, q(t), \dot{q}(t))}{\partial \dot{q}_i(t)} - \frac{\partial T(t, q(t), \dot{q}(t))}{\partial q_i(t)} + \frac{\partial U(t, q(t))}{\partial q_i(t)} = F_i(t) \quad (2)$$

where  $T$  accounts for the system’s total kinetic energy;  $U$  is the system’s total potential energy;  $t$  is the time;  $\tilde{q}$  is the generalized system degree of freedom (coordinates);  $\tilde{\dot{q}}$  is

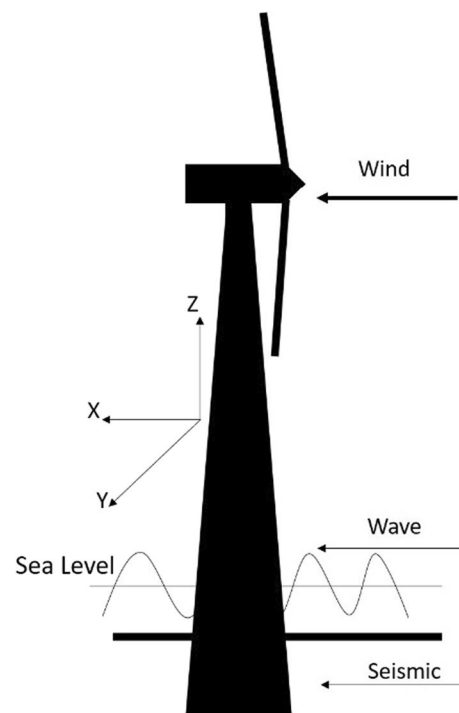


Fig. 1 Wind turbine model

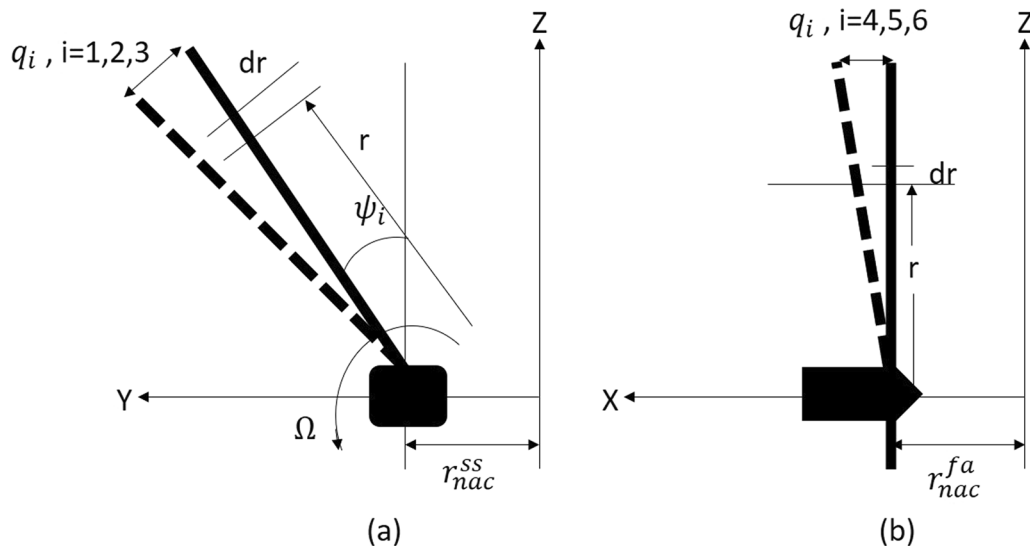


Fig. 2 Blade vibration in a edgewise direction and b flapwise direction

the first derivative w.r.t time of the generalized system degree of freedom (coordinates); and  $F$  is the generalized force vector.

2.2.1 Kinetic energy

The kinetic energy of the OWT system is given by:

$$T = T_{tow} + T_{nac} + T_f + T_{blades} \tag{3}$$

where  $T_{tow}$  represents the kinetic energy of the tower;  $T_{nac}$  denotes the kinetic energy of the nacelle;  $T_f$  denotes the kinetic energy of the foundation; and  $T_{blades}$  is the blades' kinetic energy.

The tower total absolute velocity is:

$$v_{tow} = \sqrt{v_{tow}^{fa}^2 + v_{tow}^{ss}^2} = \sqrt{(\dot{q}_7\varphi_{fa} + \dot{q}_9 + z\dot{q}_{10})^2 + (\dot{q}_8\varphi_{ss} + \dot{q}_{11} + z\dot{q}_{12})^2} \tag{4}$$

where  $z$  denotes the tower coordinate,  $\varphi_{fa}$  is the tower normalized fundamental mode shape (first mode shape) at the fore–aft direction, and  $\varphi_{ss}$  is the tower normalized fundamental mode shape (first mode shape) at the side–side direction.

Through taking an infinitesimal element  $dz$  and integrating along the tower height  $h$ , therefore  $T_{tow}$  is given by:

$$T_{tow} = \frac{1}{2} \int_0^h M_{tow,d} v_{tow}^2 dz \tag{5}$$

where  $M_{tow,d}$  represents the mass per length density of the tower.

The kinetic energy of the nacelle  $T_{nac}$  is given by:

$$T_{nac} = \frac{1}{2} M_{nac} v_{nac}^2 \tag{6}$$

where  $M_{nac}$  denotes the total mass of nacelle and hub.

The foundation's kinetic energy is  $T_f$  and given by:

$$T_f = \frac{1}{2} M_f (\dot{q}_9^2(t) + \dot{q}_{11}^2(t)) + \frac{1}{2} I_f (\dot{q}_{10}^2(t) + \dot{q}_{12}^2(t)) \tag{7}$$

where  $M_f$  and  $I_f$  are the mass of the foundation and its inertia moment, respectively.

The kinetic energy of the three blades  $T_{blades}$  is given by:

$$T_{blades} = \frac{1}{2} \sum_{i=1}^3 \int_0^R m_{blade,d} v_{blade,i}^2(r, t) dr \tag{8}$$

where  $m_{blade,d}$  denotes the mass per length density of the blades and  $R$  is the blade length. The total absolute velocity of the blade is:

$$v_{blade,i}(r, t) = \sqrt{\dot{x}_{blade,i}^2 + \dot{y}_{blade,i}^2 + \dot{z}_{blade,i}^2} \tag{9}$$

where

$$\begin{aligned}
 v_{blade,i} &= f(\dot{x}_{blade,i}, \dot{y}_{blade,i}, \dot{z}_{blade,i}) \\
 \dot{x}_{blade,i} &= v_{nac}^{ss} + \Omega r \cos(\psi_i) + \dot{q}_i \varphi_e \cos(\psi_i) - \Omega q_i \varphi_e \sin(\psi_i) \\
 \dot{y}_{blade,i} &= v_{nac}^{fa} + \dot{q}_{i+3} \varphi_f \\
 \dot{z}_{blade,i} &= -\Omega r \sin(\psi_i) - \dot{q}_i \varphi_e \sin(\psi_i) - \Omega q_i \varphi_e \cos(\psi_i)
 \end{aligned}
 \tag{10}$$

where  $\varphi_e(r)$  and  $\varphi_f(r)$  represent the normalized fundamental mode shape (first mode shape) in both edgewise direction and flapwise direction.

### 2.2.2 Potential energy

The OWT potential energy is given by:

$$U = U_{\text{tower}} + U_f + U_{\text{blades}} \tag{11}$$

where  $U_{\text{tower}}$  represents the potential energy of the tower;  $U_f$  represents the potential energy of the foundation; and  $U_{\text{blades}}$  is the potential energy of the blades.

The potential energy of the tower  $U_{\text{tower}}$  is determined by:

$$\begin{aligned}
 U_{\text{tower}} &= \int_0^h \frac{1}{2} EI(z) \left[ \frac{\partial^2 w_{fa}(z, t)}{\partial z^2} \right]^2 dz + \int_0^h \frac{1}{2} EI(z) \left[ \frac{\partial^2 w_{ss}(z, t)}{\partial z^2} \right]^2 dz \\
 U_{\text{tower}} &= \frac{1}{2} k_7 q_7^2 + \frac{1}{2} k_8 q_8^2
 \end{aligned}
 \tag{12}$$

$U_f$  is the potential energy of the foundation given by:

$$U_f = \frac{1}{2} k_x q_9^2 + \frac{1}{2} k_{xr} q_{10}^2 + \frac{1}{2} k_y q_{11}^2 + \frac{1}{2} k_{yr} q_{12}^2 \tag{13}$$

$U_{\text{blades}}$  is the potential energy of the blades owing to bending, gravity, and centrifugal stiffness in both edgewise and flapwise direction.

$$\begin{aligned}
 U_{blade,i} &= \int_0^R \frac{1}{2} EI_e(r) \left[ \frac{\partial^2 r_{ie}(r, t)}{\partial r^2} \right]^2 dr + \int_0^R \frac{1}{2} EI_f(r) \left[ \frac{\partial^2 r_{if}(r, t)}{\partial r^2} \right]^2 dr \\
 &+ \int_0^R \frac{1}{2} [-W(r)] \left( \frac{\partial r_{ie}(r, t)}{\partial r} \right)^2 dr + \int_0^R \frac{1}{2} [-W(r)] \left( \frac{\partial r_{if}(r, t)}{\partial r} \right)^2 dr \\
 &+ \int_0^R \frac{1}{2} [F_r(r)] \left( \frac{\partial r_{ie}(r, t)}{\partial r} \right)^2 dr + \int_0^R \frac{1}{2} [F_r(r)] \left( \frac{\partial r_{if}(r, t)}{\partial r} \right)^2 dr
 \end{aligned}
 \tag{14}$$

where  $W(r)$  and  $F_r(r)$  are the axial weight component and the centrifugal force along the blade, respectively.

By simplifying the blades potential energy, it can be written as:

$$U_{\text{blades}} = \frac{1}{2} \sum_{i=1}^3 [k_{ie} q_i^2 + k_{if} q_{i+3}^2] \tag{15}$$

where  $k_{ie}$  and  $k_{if}$  are the stiffness edgewise and flapwise force the  $i$ th blade, respectively.

### 2.3 Loading

The OWT is subjected to several forces as shown in the following.

#### 2.3.1 Wave turbulence loading

The water wave loading on the tower (cylindrical structure) is governed by Morison's equation [39]. To calculate the force acting on an infinitesimal element  $dz$ ,

$$dF_{\text{wave}} = \frac{\pi D^2}{4} C_M \rho \dot{u} dz + \frac{1}{2} C_D \rho D u |u| dz \tag{16}$$

$C_D$  and  $C_M$  are the drag and inertia coefficients ( $C_D=1$ ,  $C_M=1.2$ );  $\rho$  is the water density;  $D$  is the mean diameter of  $dz$ ; and  $u$  and  $\dot{u}$  are the wave velocity and acceleration of the fluid particles, respectively. Wave is dominant, uni-directional, and governed by JONSWAP spectrum [40].

$$\begin{aligned}
 S(f) &= 0.3125 H_S^2 T_p \left( \frac{f}{f_p} \right)^{-5} \exp^{-\frac{5}{4} \left( \frac{f}{f_p} \right)^{-4}} \\
 &\left( 1 - 0.287 \ln \gamma \right) \gamma^{\exp \left( -\frac{(\omega - \omega_p)^2}{2\sigma^2 \omega_p^2} \right)}
 \end{aligned}
 \tag{17}$$

where  $H_S$  denotes the significant wave height,  $f_p$  denotes the wave peak frequency  $\omega = 2\pi f$ , and  $T_p$  is the wave period  $T_p = \frac{1}{f_p}$ , in which  $\sigma = 0.07$  for  $f \leq f_p$  and  $\sigma = 0.09$  for  $f > f_p$ , where  $\sigma$  is the input parameter.

$\gamma$  is the peak parameter of the JONSWAP spectrum as follows:

$$\gamma = \begin{cases} 5 & \frac{T_p}{\sqrt{H_S}} \leq 3.6 \\ \exp \left( 5.57 - \frac{1.15 T_p}{\sqrt{H_S}} \right) & 3.6 < \frac{T_p}{\sqrt{H_S}} \leq 5 \\ 1 & \frac{T_p}{\sqrt{H_S}} < 5 \end{cases}
 \tag{18}$$

JONSWAP spectrum assumes multiple waves with different frequencies and amplitudes. To calculate

fluid particle velocity  $u$ , sum up contributions for all frequencies.

$$A_i = \sqrt{2S(\omega_i)\Delta\omega} \tag{19}$$

and

$$u(z, t) = \sum_{i=1}^N \omega_i A_i \frac{\cosh[k(z + d_w)]}{T_w \sinh(kd_w)} \sin(\omega_i t - k_i x + \theta_i) \tag{20}$$

where  $\omega$  is the wave frequency;  $k$  is the wave number;  $z$  is the coordinate as mentioned before from MSL;  $d_w$  is the water depth;  $t$  is the time;  $x$  is equal to zero; and  $\theta_i$  is a random phase angle generating and taking values from 0 to  $2\pi$ , in which  $N$  is the number of wave component of spectrum decomposition.  $k$  is calculated from the dispersion equation:

$$k \tanh(kz) = \sqrt{2S(\omega_i)\Delta\omega} \tag{21}$$

Differentiate the velocity equation to get the acceleration  $\dot{u}$ :

$$\dot{u}(z, t) = \sum_{i=1}^N \omega_i^2 A_i \frac{\cosh[k(z + d_w)]}{T_w \sinh(kd_w)} \cos(\omega_i t - k_i x + \theta_i) \tag{22}$$

Using the virtual work principle, the wave force ( $dF_{\text{wave}}$ ) acting on the virtual displacement ( $\delta u_{\text{tower}}$ ) of the immersed tower part is calculated as  $\delta W_{\text{wave}}$ .

$$\begin{aligned} \delta W_{\text{wave}} &= \int dF_{\text{wave}} \delta u_{\text{tower}} \\ &= \int dF_{\text{wave}} [\cos(\beta)(\varphi_{fa} \delta q_7 + \delta q_9 + z \delta q_{10}) \\ &\quad + \sin(\beta)(\varphi_{ss} \delta q_8 + \delta q_{11} + z \delta q_{12})] \end{aligned} \tag{23}$$

where  $\beta$  is the angle between wind and wave.

Therefore, the wave force vector is as follows:

$$F_{\text{wave}} = [0 \ 0 \ 0 \ 0 \ 0 \ 0 \ F_{7w} \ F_{8w} \ F_{9w} \ F_{10w} \ F_{11w} \ F_{12w}] \tag{24}$$

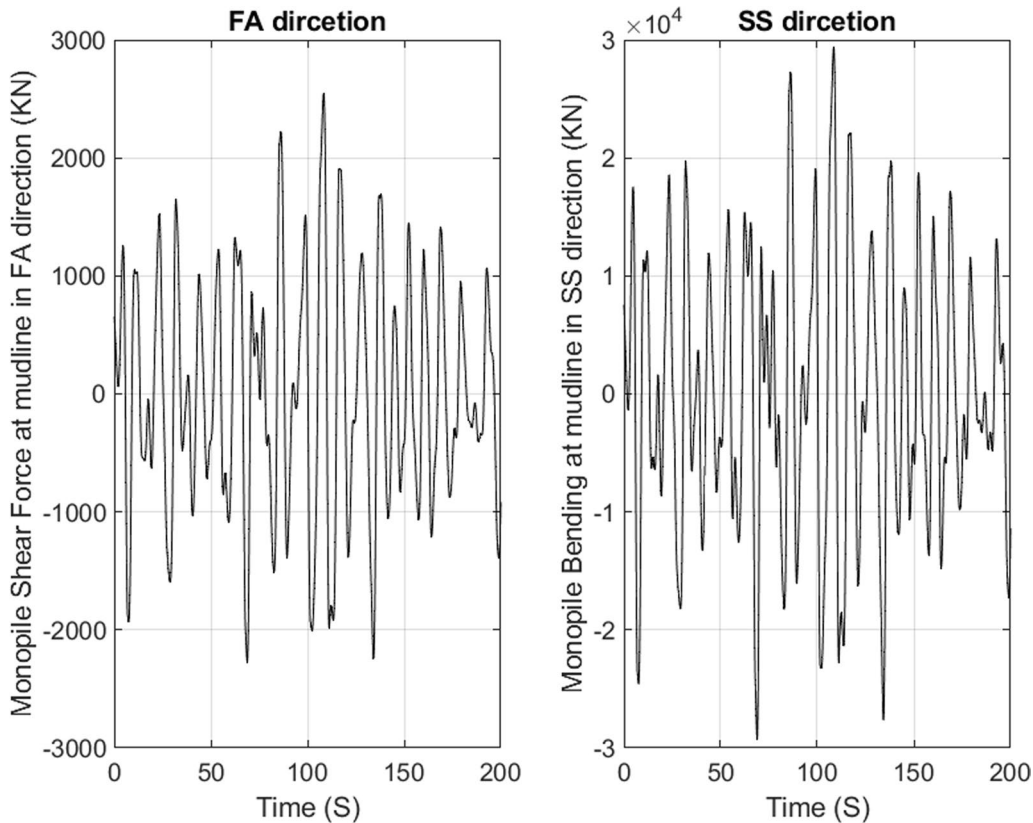


Fig. 3 Hydrodynamic load and bending loads at mudline

where

$$\begin{aligned}
 F_{7w} &= \sum_{i=1}^N \cos(\beta)A(z_i)\varphi_{fa}(z_i) & F_{8w} &= \sum_{i=1}^N \sin(\beta)A(z_i)\varphi_{fa}(z_i) \\
 F_{9w} &= \sum_{i=1}^N \cos(\beta)A(z_i) & F_{10w} &= \sum_{i=1}^N \cos(\beta)A(z_i)z_i \\
 F_{11w} &= \sum_{i=1}^N \sin(\beta)A(z_i) & F_{12w} &= \sum_{i=1}^N \sin(\beta)A(z_i)z_i \\
 A(z_i) &= \left[ \frac{\pi D^2(z_i)}{4} C_M \rho \dot{u}(z_i, t) \Delta z + \frac{1}{2} C_D \rho D(z_i) u(z_i, t) |u(z_i, t)| \Delta z \right] \quad (25)
 \end{aligned}$$

where  $\Delta z$  is the increment length.

The wave load at the mudline in fore-aft (FA) and side-side (SS) directions is shown in Fig. 3.

### 2.3.2 Aerodynamic turbulence loading

BEM derives aerodynamic force using momentum theory and local blade events. Assume constant force on each element and radial independency. Blades are divided into elements. Reference [41] applies BEM to one rotating blade element and velocities in Fig. 4.

$$\begin{aligned}
 \tan \varphi &= \frac{(1-a)V_o}{(1+\dot{a})\Omega r} \\
 \alpha &= \varphi - \theta \quad (26)
 \end{aligned}$$

In which  $V_o$  denotes the total wind speed;  $r$  represents the blade element radius;  $\Omega$  denotes the rotating blades speed;  $a$  denotes the axial velocity induction factor;  $\dot{a}$  represents the rotational velocity induction factor;  $V_{rel}$  is the relative velocity;  $\theta$  denotes the blade local pitch angle;  $\alpha$  is the angle of attack; and  $\varphi$  is the angle between the relative velocity  $V_{rel}$  and the plane of rotation (flow angle), where:

$$V_{rel} = \sqrt{((1-a)V_o)^2 + ((1+\dot{a})\Omega r)^2} \quad (27)$$

in which the drag force  $D$  and lift force  $L$  are as follows:

$$L = \frac{1}{2} \rho V_{rel}^2 c C_l & D = \frac{1}{2} \rho V_{rel}^2 c C_d \quad (28)$$

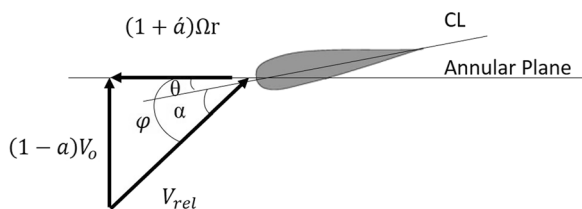


Fig. 4 Annular element of blade element with rotational and axial velocities

in which  $C_d$  represents the drag coefficient and  $C_l$  represents the lift coefficient. The plane of the blade element is concerning with tangential  $F_T$  and normal  $F_N$  forces, respectively.

$$\begin{aligned}
 F_T &= L \sin \varphi - D \cos \varphi \\
 F_N &= L \cos \varphi + D \sin \varphi \quad (29)
 \end{aligned}$$

According to the above equations, the axial  $a$ , rotational  $\dot{a}$  velocity induction factor, and total wind speed  $V_o$  are required. Firstly, the induction factors are obtained from the algorithm stated in eight steps in Ref. [50] and through the definitions.

$$\begin{aligned}
 a &= \frac{1}{\frac{4 \sin^2 \varphi}{\sigma C_n} + 1} \\
 \dot{a} &= \frac{1}{\frac{4 \sin \varphi \cos \varphi}{\sigma C_t} - 1} \quad (30)
 \end{aligned}$$

where  $\sigma$  is the solidity and  $C_n$  is the normal coefficient and  $C_t$  is the tangential coefficient, which are expressed as:

$$\begin{aligned}
 C_n &= C_l \cos \varphi + C_d \sin \varphi \\
 C_t &= C_l \sin \varphi - C_d \cos \varphi \quad (31)
 \end{aligned}$$

Equations from (26) to (31) are obtained from Ref. [41]. Secondly, the total wind speed  $V_o$  is;

$$V_o(z, t) = V_{mean}(z) + V_{turb}(t) \quad (32)$$

where  $V_{mean}(z)$  is the mean velocity which is constant and depending consequently on the height  $z$  according to the equation of Log Wind Profile:

$$V_{mean}(z) = u_{hub} \frac{\log \frac{z}{z_o}}{\log \frac{h_{hub}}{z_o}} \quad (33)$$

where  $u_{hub}$  represents the wind velocity at reference length  $h_{hub}$  which is the hub length or top tower length and  $z_o$  is the roughness length and its value is 0.03.

The turbulent wind velocity  $V_{turb}(t)$  term is obtained through von Karman spectrum model Ref. [42]. The spectral model is:

$$S_u(f) = \frac{4\sigma_u^2 \frac{L}{u_{hub}}}{\left(1 + 71 \left(\frac{fL}{u_{hub}}\right)^2\right)^{\frac{5}{6}}} \quad (34)$$

and

$$S_{v,w}(f) = \frac{2\sigma_{v,w}^2 \frac{L}{u_{hub}}}{\left(1 + 71\left(\frac{fL}{u_{hub}}\right)^2\right)^{\frac{11}{6}}} \left(1 + 189\left(\frac{fL}{u_{hub}}\right)^2\right) \tag{35}$$

in which  $L$ ,  $f$ , and  $\sigma$  are integral scale parameter; cyclic frequency, and standard deviation, respectively. The integral scale parameter is defined by the turbulence scale parameter  $\Lambda_v$  by:

$$L = 3.5\Lambda_v \tag{36}$$

where

$$\sigma_u = \sigma_v = \sigma_w \tag{37}$$

$$\delta W_{Aero} = \sum_{i=1}^3 \left[ \int_0^R F_{Ni}(r, t) \left\{ \varphi_{fa} \delta q_{i+3} + \delta r_{nac}^{fa} \right\} dr + \int_0^R F_{Ti}(r, t) \left\{ \varphi_{ss} \delta q_i \cos(\psi_i) + \delta r_{nac}^{ss} \right\} dr \right] \tag{38}$$

Therefore, the aero force vector is as follows:

$$F_{Aero,i} = \frac{\partial(\delta W_{Aero})}{\partial(\delta q_i)} \tag{39}$$

$$F_{Aero} = [F_{1A} \ F_{2A} \ F_{3A} \ F_{4A} \ F_{5A} \ F_{6A} \ F_{7A} \ F_{8A} \ F_{9A} \ F_{10A} \ F_{11A} \ F_{12A}] \tag{40}$$

where

$$F_{iA} = \int_0^R F_{Ti}(r, t) \varphi_{ss,i} dr \ \& \ F_{(i+3)A} = \int_0^R F_{Ni}(r, t) \varphi_{fa,i} dr, \quad i = 1, 2, 3$$

$$F_{7A} = F_{9A} = \sum_{i=1}^3 \left[ \int_0^R F_{Ni}(r, t) dr \right] \ \& \ F_{8A} = F_{11w} = \left[ \sum_{i=1}^3 \int_0^R F_{Ti}(r, t) \sin(\psi_i) dr \right]$$

$$F_{10w} = h \sum_{i=1}^3 \left[ \int_0^R F_{Ni}(r, t) dr \right] \ \& \ F_{12w} = h \sum_{i=1}^3 \left[ \int_0^R F_{Ti}(r, t) \sin(\psi_i) dr \right] \tag{41}$$

The relative velocity of the wind on a fixed position of one rotor blade, with a radial position of 48 m away from the hub center, is compared to HAWC2 code simulation [43] with a mean wind speed of 11 m/s as demonstrated in Fig. 5.

To determine the aerodynamic force vector, virtual work principle is applied in which virtual work  $\delta W_{Aero}$  of wind force acted by wind force  $dF_{Aero}$  on the virtual displacement  $\delta u$  as follows:

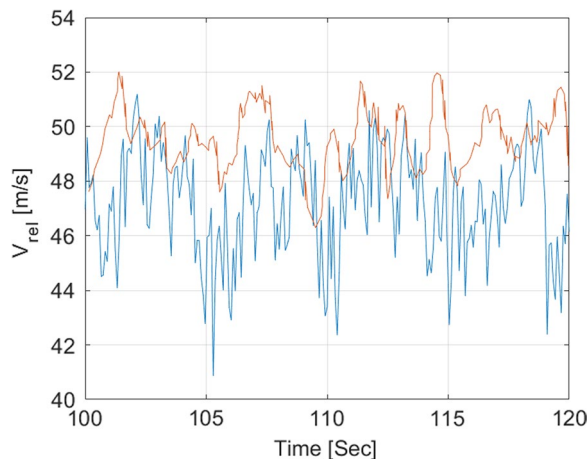


**Fig. 5** The blade 1 relative velocity at a radial position of 48 m away from the hub center compared to HAWC2 code simulation

### 2.3.3 Solution of the nonlinear equation of motion

Recalling equation (2) and substituting the kinetic and potential energy and differentiate, the following nonlinear equation is obtained:

$$[M]\ddot{q} + [C]\dot{q} + [K]q = F_{wave} + F_{Aero} \tag{42}$$

Equation (42) is nonlinear with time-varying terms, involving stiffness matrices  $[K]$ , mass matrix  $[M]$ , damping matrix  $[C]$ , and degrees of freedom vector  $q$  and its derivatives  $\dot{q}$  and  $\ddot{q}$ . It also includes force vectors  $F_{wave}$ ,  $F_{Seismic}$ , and  $F_{Aero}$  for wave, seismic, and aerodynamic forces, respectively. The Newmark integration scheme [44] is used to solve it, and the results are presented in the next section.

## 3 Results

### 3.1 Comparative study

The numerical model is verified with the NREL 5 MW wind turbine [43, 45] phase 2, with soil–structure interaction SSI properties according to Ref. [46], in which the longitudinal stiffness in both x and y directions is  $K_{lx} = K_{ly} = 2.574E6$  KN/m; the rotational stiffness in both x and y directions is  $K_{rx} = K_{ry} = 2.629E8$  KN/rad; stiffness in coupled direction is  $K_{xy} = -2.253E7$  KNm/m; the longitudinal damping ratio in both x and y directions is  $\zeta_{lx} = \zeta_{ly} = 0.6\%$ ; the rotational damping ratio in both x and y directions is  $\zeta_{rx} = \zeta_{ry} = 0.6\%$ ; the blade damping

**Table 1** Natural frequencies of FAST and nonlinear model

	FAST	Presented model	Error %
First tower FA freq. (Hz)	0.25	0.2502	0.0982
First tower SS freq. (Hz)	0.25	0.2502	0.0982
First blade edgewise freq. (Hz)	1.079	1.0941	1.4020
First blade flapwise freq. (Hz)	0.668	0.6723	0.6404

ratio in FA and SS is  $\zeta_{bFF} = \zeta_{bSS} = 0.48$ ; and the tower damping ratio in FA and SS is  $\zeta_{TF} = \zeta_{TSS} = 1\%$ .

The comparison of the natural frequencies of the presented nonlinear model with FAST in which a great agreement is obtained is given in Table 1.

**Comparison** First fundamental frequencies—tower and blade in static conditions (FA and SS). Tower: identical frequencies (0.1% error). Blade: around 1% higher than FAST program, consistent with other models [].

The hydrodynamic response is validated with all simulation models in the technical report [43] and matches with all of them in the following.

Table 2 compares the translation displacement at the mudline in meters and the rotational displacement in radians resulting from the hydrodynamic loads on the monopile. The results from two models, namely NREL FAST CS and CENER FAST CS, are compared to the results obtained from the modified model. The comparison indicates a strong alignment between the results from the modified model and those from the other two models.

Table 3 displays the results of the blade’s steady-state response under aerodynamic loads, and these results are compared to those obtained from the FAST model. The comparison demonstrates a strong agreement between the findings of the two models.

**3.2 Hydrodynamic (wave) and aerodynamic (wind) loads effect**

For  $\beta = 0^\circ$ , wind speed of 11.4 m/s and the rotating blades with 12.1 rpm, the wind turbine responses for the acceleration and displacement are shown below, and the response is presented for blade in the FA and SS directions in Fig. 6.

**Table 3** The blade flap wise steady-state response

	Presented model	FAST
Flapwise blade tip displacement (m)	5.52	5.65

Figure 6 focuses on the blade’s acceleration and displacement response, in which the acceleration in the FA direction is greater than the acceleration in the SS direction.

Figure 7 illustrates the acceleration and displacement responses of the tower. Notably, in the fore–aft (FA) direction, the response dominates (details to be discussed later). In this FA direction, the acceleration oscillates around zero, while the displacement predominantly fluctuates in the positive direction. This indicates that the displacement continuously oscillates about a positive value due to the continuous airflow in this direction. Furthermore, in the FA direction, the acceleration is significantly larger than in the side–side (SS) direction. Additionally, the displacement and acceleration exhibit values of approximately the same magnitude in this direction.

In Table 4, the mean displacement for blade and nacelle in the FF and SS directions for different  $\beta$  is given, where  $q_1$  is the displacement of the first blade in the SS direction;  $q_4$  displacement of the first blade in the FA direction;  $q_7$  displacement of the nacelle in the FA direction;  $q_8$  displacement of the nacelle in the SS direction;  $r_{nac}^{fa}$  the tower absolute displacement in FA direction; and  $r_{nac}^{ss}$  the absolute displacement of the tower in side–side direction.

The various values of  $\beta$  represent the direction of wave forces. It is worth noting that the impact of the wave loads primarily influences the side–side (SS) direction. This explains why the values for the SS direction in the tower are generally of smaller magnitude compared to the fore–aft (FA) direction.

The calculated responses indicate that:

The maximum displacement of the tower in the FA direction is reduced by 42% due to the misalignment of forces.

The maximum displacement of the tower in the SS direction is significantly affected by changes in direction,

**Table 2** Monopile displacement of two different models and the presented one

	Presented model	NREL FAST CS	CENER FAST CS
Min. monopile translation displacement at mudline (m)	−0.0164	−0.0131	−0.0161
Max. monopile translation displacement at mudline (m)	0.0176	0.0171	0.0196
Min. monopile rotational displacement at mudline (rad)	−0.1016	−0.097	−0.110
Max. monopile rotational displacement at mudline (rad)	0.1081	0.101	0.121

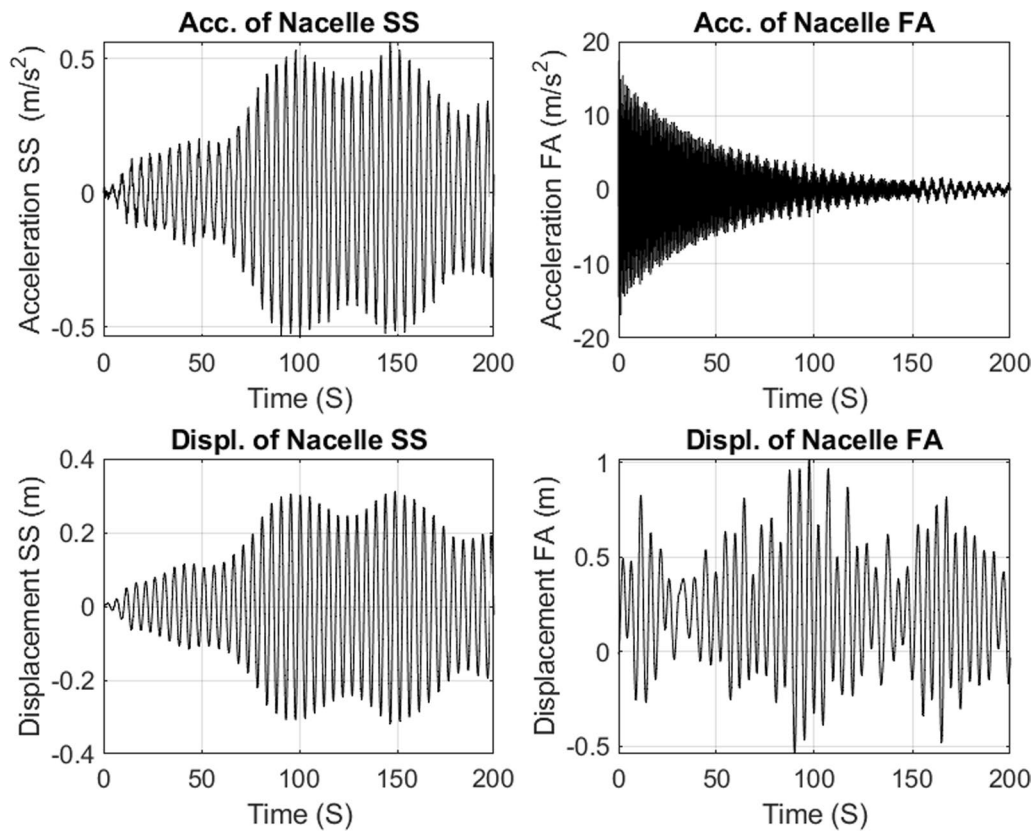


**Fig. 6** The blade acceleration and displacement response

with an increase of approximately 140% between no misalignment and a complete change in direction by  $90^\circ$  for wave loads.

For the blades, the maximum displacement in both the SS and FA directions shows slight changes between no misalignment and a complete change in direction by  $90^\circ$  for both wave loads.

The mean displacement remains unaffected by misalignment, while the maximum values are significantly altered due to misalignment for the tower only.

### 3.3 Effect of variable cross section

The following table shows the effect of variable cross of wind turbine tower for  $\beta = 90^\circ$ .

Table 5 shows the significant effect: variable cross-sectional tower vs. constant cross section. Nacelle FA displacement: 15–16% error at  $\beta=0^\circ$ , ~18% increased relative displacement. Nacelle SS displacement: 8–9% error. Blades: <1% error in SS, almost zero error in FA. Constant cross-sectional overestimates displacement.

## 4 Discussion

In this study, we have undertaken the development of a sophisticated multi-degree-of-freedom (MDOF) model tailored for offshore wind turbine towers. This model is distinct in its consideration of towers with non-uniform cross sections and flexible foundations. The core components of our model encompass the intricate interactions between the tower, nacelle, and blades, as well as the dynamic coupling between the structure and the seabed, a relationship we have represented using a combination of springs and dampers. We have also paid close attention to the complex dynamics of the turbine blades, taking into account centrifugal forces, bending stiffness, and the influence of gravity on their behavior. To simulate the impact of ocean waves, we have employed the renowned Morison equation, complemented by the Joint North Sea Wave Project (JONSWAP) spectrum for side-side (SS) direction loading.

Our results, as presented before, shed light on the mean displacement values for both the blade and nacelle in the fore-aft (FA) and SS directions across a range of  $\beta$  angles.

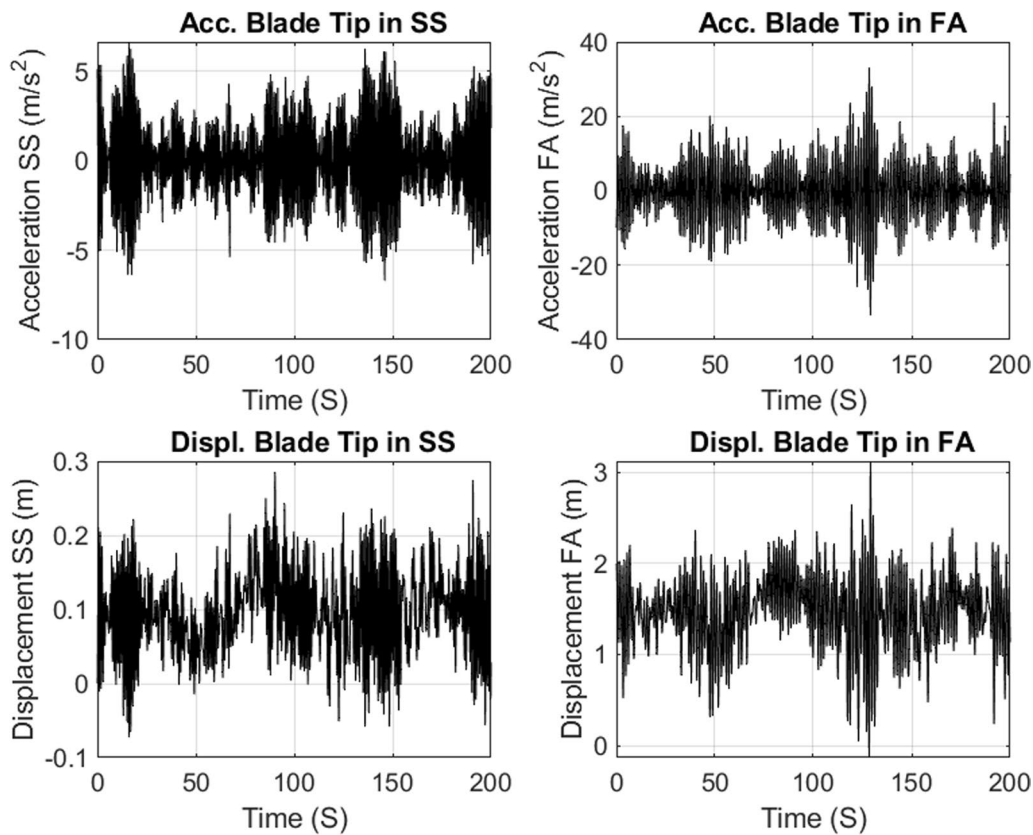


Fig. 7 The Nacelle acceleration and displacement response

Table 4 The mean displacement for blade and nacelle in the FF and SS directions for different  $\beta$

	$q_1$ (m)	$q_4$ (m)	$q_7$ (m)	$q_8$ (m)	$r_{nac}^{fa}$ (m)	$r_{nac}^{ss}$ (m)
$\beta = 0^\circ$	0.0968	1.4756	0.2221	6.9e-4	0.2525	7.9e-4
$\beta = 30^\circ$	0.0955	1.4756	0.2222	4.1e-4	0.2526	4.3e-4
$\beta = 60^\circ$	0.0946	1.4757	0.2224	1.7e-4	0.2529	2.0e-4
$\beta = 90^\circ$	0.0942	1.4758	0.2227	8.1e-5	0.2533	1.3e-4

Table 5 Worthiness of variable cross-sectional consideration

Location	Variable CS (m)	Constant CS (m)	Error %
Blade tip in FA direction	1.4758	1.4759	-0
Blade tip in SS direction	0.0942	0.0944	0.21
Nacelle in FA direction	0.2533	0.2140	15.5
Nacelle in SS direction (Max.)	0.8544	0.7792	8.8
$q_7$	0.2227	0.1834	17.6
$q_8$ (Max.)	0.7100	0.6321	12.32

Upon meticulous examination of our findings, it becomes evident that the maximum displacement of the tower in the SS direction is profoundly influenced by

variations in  $\beta$ . We observe a striking approximate 140% increase in displacement when transitioning from a scenario of no misalignment to a scenario involving a complete  $90^\circ$  change in direction with regard to wave loads.

In contrast, the blade’s maximum displacement values in both the SS and FA directions exhibit only marginal variations when comparing the no misalignment scenario to a complete  $90^\circ$  change in direction for wave loads. The overall conclusion here is that blade displacement remains relatively stable in the face of misalignment.

It is essential to underline that while the mean displacement of the system remains comparatively consistent across various misalignment scenarios, the most significant shifts are concentrated within the tower’s

response. These fluctuations in tower displacement serve as a vital point of consideration for structural engineers and designers.

In summary, our research has offered a deep insight into the intricate dynamics of offshore wind turbine towers. It elucidates the profound impact that different orientations and misalignments can have on structural behavior. These findings hold considerable significance for the offshore wind energy sector, impacting tower design and structural integrity. This study underscores the need for further research aimed at devising strategies to mitigate the impact of misalignment on tower displacement, with a broader objective of enhancing the overall performance and safety of offshore wind turbines.

## 5 Conclusion

A modified multi-degree-of-freedom (MDOF) model has been developed to analyze offshore wind turbine towers with varying cross sections and elastic foundations. This model accounts for the interaction between the tower, nacelle, and blades in both the fore–aft (FA) and side–side (SS) directions. The interaction between the structure and the soil is represented using longitudinal and rotational springs and dampers in both FA and SS directions. Blade dynamics are incorporated in the model by considering centrifugal stiffness, bending stiffness, and gravity. Wave loads are calculated using the Morison equation, with wave data generated from the JONSWAP spectrum. Aerodynamic loads are determined using the blade element moment theory, and the wind spectrum is generated using the Von Karman spectrum. The non-linear governing equations are derived using an Euler–Lagrangian energy-based method and solved using the Newmark method. The primary objective of this study is to quantitatively assess the impact of varying cross-sectional shapes of wind turbine towers on the simulated response values of the real NREL 5 MW offshore wind turbine. The results of this study indicate that simulating the tower with varying cross sections, as opposed to assuming a constant cross section, can have significant implications. The error increases by 20% when a constant cross-sectional assumption is applied. The study systematically examines the response of the offshore wind turbine to various load types and different misalignments of wave and seismic loads with aerodynamic loads, presenting a detailed analysis of the results.

## 6 Recommendations

- The tower can be modeled as viscoelastic material instead of flexible foundations.

- New numerical techniques can be used as mentioned in Ref. [47–52] in its stability as in Ref. [53].

### Abbreviations

MW	Mega watt
NREL	National Renewable Energy Laboratory
OWT	Offshore wind turbines
DQM	Differential quadrature method
KW	Kilo watt
SDOF	Single-degree-of-freedom
STMD	Semi-active tuned mass dampers
MDOF	Multi-degree-of-freedom
MTMD	Multiple tuned mass damper
ATMD	Active tuned mass damper
CFD	Computational fluid dynamics
SSI	Soil–structure interaction
$\beta$	Wind–wave misalignment angle
$\Omega$	Rotating blades angle
$\psi_i$	Blades angle of the $i$ th blade
$q_1$ – $q_3$	Edgewise coordinates
$q_4$ – $q_6$	Flapwise coordinates
$q_7$	Fore–aft nacelle's relative motion DOF
$q_8$	Side–side nacelle's relative motion DOF
$q_9$ – $q_{11}$	Translational SSI DOF
$q_{10}$ – $q_{12}$	Rotational SSI DOF
$k_{lx}$ – $k_{ly}$	Two translational springs modeling SSI
$k_{rx}$ – $k_{ry}$	Two rotational springs modeling SSI
$k_{xy}$	Coupled spring modeling SSI
$c_{lx}$ – $c_{ly}$	Two translational dashpot dampers modeling SSI
$c_{rx}$ – $c_{ry}$	Two rotational dashpot dampers modeling SSI
$\tilde{q}$	Generalized system DOF w.r.t
$\dot{\tilde{q}}$	First derivative of generalized system DOF w.r.t
$T$	System kinetic energy
$U$	System potential energy
$F$	Generalized force vector
$T_{\text{tow}}$	Kinetic energy of the tower
$T_{\text{nac}}$	Kinetic energy of the nacelle
$T_f$	Kinetic energy of the foundation
$T_{\text{blades}}$	Kinetic energy of the blades
$U_{\text{tow}}$	Potential energy of the tower
$U_f$	Potential energy of the foundation
$U_{\text{blades}}$	Potential energy of the blades
$F_{\text{wave}}$	Wave force vector
$F_{\text{Aero}}$	Aero force vector

### Acknowledgements

Not applicable.

### Author contributions

TMH team leader initiated the concept of the paper. MAEA derived the governing equations, applied the numerical technique, got the results, and wrote the manuscript. ZE and HHI checked out the results and manuscript. All authors have read and approved the manuscript.

### Funding

Not applicable.

### Availability of data and materials

Not applicable.

### Declarations

### Ethics approval and consent to participate

Not applicable.

**Consent for publication**

Not applicable.

**Competing interests**

The authors declare that they have no competing interests.

Received: 3 August 2023 Accepted: 1 November 2023

Published online: 11 November 2023

**References**

- Thresher RW (2009) Structural dynamic analysis of wind turbine systems. *J Sol Energy Eng* 104(2):89–95. <https://doi.org/10.1115/1.3266291>
- Halfpenny A (1998) Dynamic analysis of both on and offshore wind turbines in the frequency domain. University College London, London
- Ahlström A (2002) Simulating dynamical behavior of wind power structures (Stockholm). Technical Report
- Kessentini S, Choura S, Najjar F, Franchek MA (2010) Modeling and dynamics of a horizontal axis wind turbine. *J Vib Control* 16(13):2001–2021. <https://doi.org/10.1177/1077546309350189>
- Molenaar DP, Tempel DP (2002) Wind turbine structural dynamics—a review of the principles for modern power generation, onshore and offshore. *Wind Eng* 26:211–220. <https://doi.org/10.1260/030952402321039412>
- Oh K-Y, Nam W, Ryu MS, Kim J-Y, Epureanu BI (2018) A review of foundations of offshore wind energy converters: current status and future perspectives. *Renew Sustain Energy Rev* 88:16–36. <https://doi.org/10.1016/j.rser.2018.02.005>
- Xu Y et al (2008) Static and dynamic analysis of wind turbine tower structure. *Adv Mater Res* 33–37:1169–1174. <https://doi.org/10.4028/www.scientific.net/AMR.33-37.1169>
- Bhattacharya S, Cox J, Lombardi D, Muir Wood D (2012) Dynamics of offshore wind turbines supported on two foundations. *Proc ICE-Geotech Eng* 166:159–169. <https://doi.org/10.1680/geng.11.00015>
- Adhikari S, Bhattacharaya S (2011) Vibrations of wind-structures considering soil-structure interaction. *Wind Struct* 14(2):85–112. <https://doi.org/10.12989/was.2011.14.2.085>
- Bhattacharaya S, Adhikari S (2011) Experimental validation of soil-structure interaction of offshore wind turbines. *Soil Dyn Earthq Eng* 31:805–816. <https://doi.org/10.1016/j.soildyn.2011.01.004>
- Arany L, Bhattacharya S, Adhikari S, Hogan SJ, Macdonald JHG (2015) An analytical model to predict the natural frequency of offshore wind turbines on three-spring flexible foundations using two different beam models. *Soil Dyn Earthq Eng* 74:40–45. <https://doi.org/10.1016/j.soildyn.2015.03.007>
- Alamo GM, Aznárez JJ, Padrón LA, Martínez-Castro AE, Gallego R, Maeso O (2016) Dynamic response of real offshore wind turbines on monopiles in stratified seabed. In: ECCOMAS congress. <https://doi.org/10.7712/100016.2117.6772>
- Tayesh K, Nasar T (2016) Prediction of natural frequency of wind turbine off Mangalore coast international. *J Innov Res Sci Eng Technol* 5(9)
- Wang S, Huang Y, Li L, Liu C, Zhang D (2017) Dynamic analysis of wind turbines including nacelle–tower–foundation interaction for condition of incomplete structural parameters. *Adv Mech Eng* 9(3):1–17. <https://doi.org/10.1177/1687814017692940>
- Bouzid DA, Bhattacharya S, Otsmane L (2018) Assessment of natural frequency of installed offshore wind turbines using nonlinear finite element model considering soil-monopile interaction. *J Rock Mech Geotech Eng*. <https://doi.org/10.1016/j.jrmge.2017.11.010>
- Negm HM, Maalawi KY (2000) Structural design optimization of wind turbine towers. *Comput Struct* 74:649–666. [https://doi.org/10.1016/S0045-7949\(99\)00079-6](https://doi.org/10.1016/S0045-7949(99)00079-6)
- Murtagh PJ, Basu B, Broderick BM (2005) Along-wind response of a wind turbine tower with blade coupling subjected to rotationally sampled wind loading. *Eng Struct* 27:1209–1219. <https://doi.org/10.1016/j.engstruct.2005.03.004>
- AlHamaydeh M, Hussain S (2011) Optimized frequency-based foundation design for wind turbine tower utilizing soil–structure interaction. *J Frankl Inst* 348:1470–1487. <https://doi.org/10.1016/j.jfranklin.2010.04.013>
- Arrigan J et al (2011) Control of flapwise vibrations in wind turbine blades using semi-active tuned mass dampers. *Struct Control Health Monit* 18:840–851. <https://doi.org/10.1002/stc.404>
- Arturo Soriano L, Yu W, Jesus Rubio JD (2013) Modeling and control of wind turbine. *Math Probl Eng* 2013
- Liu WY (2013) The vibration analysis of wind turbine blade–cabin–tower coupling system. *Eng Struct* 56:954–957. <https://doi.org/10.1016/j.engstruct.2013.06.008>
- Genov J et al (2010) Modeling and control of wind turbine tower vibrations. In: Conference Paper May 2010. <https://doi.org/10.1063/1.3515600>
- Fitzgerald B, Basu B (2016) Structural control of wind turbines with soil structure interaction included. *Eng Struct* 111:131–151. <https://doi.org/10.1016/j.engstruct.2015.12.019>
- Zuo H, Bi K, Hao H (2017) Using multiple tuned mass dampers to control offshore wind turbine vibrations under multiple hazards. *Eng Struct* 141:303–315. <https://doi.org/10.1016/j.engstruct.2017.03.006>
- Staino A, Basu B (2015) Emerging trends in vibration control of wind turbines: a focus on a dual control strategy. *Philos Trans R Soc A* 373:20140069. <https://doi.org/10.1098/rsta.2014.0069>
- Mohammadi E, Fadaeinedjad R, Moschopoulos G (2018) Implementation of internal model based control and individual pitch control to reduce fatigue loads and tower vibrations in wind turbines. *J Sound Vib* 421:132–152. <https://doi.org/10.1016/j.jsv.2018.02.004>
- Hussan M et al (2018) Multiple tuned mass damper for multi-mode vibration reduction of offshore wind turbine under seismic excitation. *Ocean Eng* 160:449–460. <https://doi.org/10.1016/j.oceaneng.2018.04.041>
- Sun C (2018) Semi-active control of monopile offshore wind turbines under multi-hazards. *Mech Syst Signal Process* 99:285–305. <https://doi.org/10.1016/j.ymssp.2017.06.016>
- Hemmati A, Oterkus E (2018) Semi-active structural control of offshore wind turbines considering damage development. *J Mar Sci Eng* 6:102. <https://doi.org/10.3390/jmse6030102>
- Brodersen ML, Bjørke A-S, Høgsberg JB (2017) Active tuned mass damper for damping of offshore wind turbine vibrations. *Wind Energy* 20(5):783–796. <https://doi.org/10.1002/we.2063>
- Hsu M-H (2007) Dynamic behaviour of wind turbine blades. *J Mech Eng Sci*. Doi: <https://doi.org/10.1243/09544066JMES759>
- Park J-H et al (2010) Linear vibration analysis of rotating wind-turbine blade. *Curr Appl Phys* 10:S332–S334. <https://doi.org/10.1016/j.cap.2009.11.036>
- Li L et al (2014) A mathematical model for horizontal axis wind turbine blades. *Appl Math Model* 38:2695–2715. <https://doi.org/10.1016/j.apm.2013.10.068>
- Kono T et al (2016) Numerical analysis of the effects of a wind turbine's rotating blades on the aerodynamic forces on the tower. In: First international symposium on flutter and its application. <https://doi.org/10.3390/en10010121>
- El Mouhsine S et al (2017) Aerodynamics and structural analysis of wind turbine blade. *Procedia Manuf* 22:747–756. <https://doi.org/10.1016/j.promfg.2018.03.107>
- Júnior CJF et al (2019) Modeling wind turbine blades by geometrically-exact beam and shell elements: a comparative approach. *Eng Struct* 180:357–378. <https://doi.org/10.1016/j.engstruct.2018.09.032>
- El Absawy MA, Elnaggar Z, Ibrahim HH (2019) Dynamic behavior of variable cross-section offshore wind turbine with flexible foundation using finite element method. *J Phys Conf Ser*. <https://doi.org/10.1088/1742-6596/1264/1/012048>
- El Absawy MA, Elnaggar Z, Ibrahim HH (2019) Semi analytical model for the dynamic behavior of offshore wind turbine with flexible foundation. *J Phys Conf Ser*. <https://doi.org/10.1088/1742-6596/1264/1/012049>
- Faltinsen OM (1990) Sea loads on ships and offshore structures. Cambridge University Press, Cambridge
- Hasselmann K, Barnett T, Bouws E, Carlson H, Cartwright D, Enke K, Ewing J, Gienapp H, Hasselmann D, Kruseman P, Meerburg A, Muller P, Olbers D, Richter K, Sell W, Walden H (1973) Measurements of wind-wave growth

and swell decay during the Joint North Sea Wave Project (JONSWAP). *Deut Hydrogr Z* 8:1–95

41. Hansen MOL (2000) *Aerodynamics of wind turbines*. James & James (Science Publishers) Ltd.
42. Jonkman BJ, Buhl ML, Jr. (2006) *TurbSim user's guide*. United States: N. p., 2006. Web. <https://doi.org/10.2172/891594>
43. Jonkman J, Musial W (2010) Offshore code comparison collaboration (OC3) for IEA Task 23 offshore wind technology and deployment. Technical Report NREL/TP-5000-48191; National Renewable Energy Laboratory (NREL): Golden, CO, USA
44. Bathe K-J (2014) *Finite element procedures*, 2nd edn. K. J. Bathe, Watertown, Ch. 9, pp 777–779
45. Jonkman J, Butterfield S, Musial W, Scott G (2009) Definition of a 5-MW reference wind turbine for offshore systems development technical report NREL
46. Carswell W, Johansson J, Lovholt F, Arwade SR, Madshus C, DeGroot DJ, Myers AT (2015) Foundation damping and the dynamics of offshore wind turbine monopiles. *Renew Energy* 80:724–736. <https://doi.org/10.1016/j.renene.2015.02.058>
47. Mahdy AMS, Babatin MM, Khader MM (2022) Numerical treatment for processing the effect of convective thermal condition and Joule heating on Casson fluid flow past a stretching sheet. *Int J Mod Phys*. <https://doi.org/10.1142/S012918312250108X>.
48. Ahmed HF, Melad MB (2023) A new numerical strategy for solving nonlinear singular Emden-Fowler delay differential models with variable order. *Math Sci* 17:399–413. <https://doi.org/10.1007/s40096-022-00459-z>
49. Mahdy A, Mohamed M, Lotfy K, Alhazmi M, El-Bary A, Raddadi MH (2021) Numerical solution and dynamical behaviors for solving fractional nonlinear Rubella ailment disease model. *Results Phys*. <https://doi.org/10.1016/j.rinp.2021.104091>
50. Mahdy AMS, Gepreel KA, Al-Azab K, El-Bary AA (2021) A numerical method for solving the Rubella ailment disease model. *Int J Mod Phys C* 32(7):2150097. <https://doi.org/10.1142/S0129183121500972>
51. Mahdy AMS, Abdou MA, Mohamed DS (2023) Computational methods for solving higher-order (1+1) dimensional mixed-difference integro-differential equations with variable coefficients. *Mathematics* 11(9): 2045. <https://doi.org/10.3390/math11092045>
52. Amer YA, Mahdy AMS, Namoos HAR (2018) Reduced differential transform method for solving fractional-order biological systems. *J Eng Appl Sci* 13:8489–8493. <https://doi.org/10.36478/jeasci.2018.8489.8493>
53. Mahdy A (2023) Stability, existence, and uniqueness for solving fractional glioblastoma multiforme using a Caputo-Fabrizio derivative. *Math Methods Appl Sci*. <https://doi.org/10.1002/mma.9038>

## Publisher's Note

Springer Nature remains neutral with regard to jurisdictional claims in published maps and institutional affiliations.

Submit your manuscript to a SpringerOpen<sup>®</sup> journal and benefit from:

- Convenient online submission
- Rigorous peer review
- Open access: articles freely available online
- High visibility within the field
- Retaining the copyright to your article

---

Submit your next manuscript at ► [springeropen.com](https://www.springeropen.com)

---